applied sciences

MDPI

Article

Micro-Structured Patches for Dermal Regeneration Obtained via Electrophoretic Replica Deposition

Arash Ghalayani Esfahani [1], Lina Altomare [1,2], Lorenzo Bonetti [1,2], Fereshteh Nejaddehbashi [3], Francesca Boccafoschi [4], Roberto Chiesa [1,2], Federica Boschetti [1], Vahid Bayati [3] and Luigi De Nardo [1,2,*]

1 Department of Chemistry, Materials and Chemical Engineering 'G. Natta', Politecnico di Milano, 20133 Milan, Italy; arash.ghalayani@polimi.it (A.G.E.); lina.altomare@polimi.it (L.A.); lorenzo.bonetti@polimi.it (L.B.); roberto.chiesa@polimi.it (R.C.); Federica.boschetti@polimi.it (F.B.)
2 INSTM—National Interuniversity Consortium of Materials Science and Technology, 50121 Firenze, Italy
3 Cellular and Molecular Research Center (CMRC), Ahvaz Jundishapur University of Medical Sciences, Ahvaz Khuzestan 61357-15794, Iran; fereshte_negad@yahoo.com (F.N.); bayati-v@ajums.ac.ir (V.B.)
4 Department of Health Sciences, University of Piemonte Orientale, 28100 Novara, Italy; Francesca.boccafoschi@med.uniupo.it
* Correspondence: luigi.denardo@polimi.it; Tel.: +39-0223993161

Received: 14 May 2020; Accepted: 17 July 2020; Published: 21 July 2020

Abstract: Artificial substrates supporting the healing of skin wounds require specific structural and chemical architectures that promote a recapitulation of the complexity of the native organ. Bottom-up fabrication technologies are emerging as effective strategies to fine tune biochemical, morphological, and structural features intended for regenerative applications. Here, we proposed an electrophoretic replica deposition (EPrD) approach to realize chitosan three-dimensional structures specifically designed to treat patients with serious cutaneous damages or losses. The EPrD process has been optimized to consistently obtain random porosity vs. hierarchical lattice structures, showing mechanical properties in the range of skin tissue (E = 0.2–20 MPa). The obtained patches were tested in vivo via a one-stage grafting procedure in a full thickness skin wound rat model. Chitosan patches showed no adverse reactions throughout the experimental period (14 days). Hair follicles and sebaceous glands were observed in histological sections, indicating the regeneration of a thin epidermal layer with more skin appendages. Immunohistochemistry results demonstrated that keratin 10 was mostly expressed in basal and suprabasal layers, like normal skin, in structures with random porosity and with smaller lattice structures. The obtained results show the potential of EPrD to innovate the design of artificial substrates in skin healing therapies.

Keywords: chitosan; biopolymers; wound healing; electrophoretic replica deposition (EPrD); in vivo test; bottom-up technology

1. Introduction

The wound management of severe skin damage or loss is a clinical procedure required by a significant number of people who suffer from chronic diseases or have been involved in traumatic events [1]. Cutaneous wound regeneration remains a critical procedure for the treatment of those patients in which injuries compromising the integrity and the protective functions of skin would result in physiologic imbalance, relevant disability, or even death [2]. The healing of a skin wound is a complex phenomenon that

includes a wide range of molecular, cellular, physiological, and biological processes: a deep understanding of the intricate cascade of events taking place during skin repair [3] offers fundamental guidelines for the design of wound dressings. Many skin substitutes, and a relevant number of solutions, have been developed so far to target wound healing processes by creating a suitable local micro-environment at the site of implant [4]. The ideal goal of a skin substitute is to rapidly produce a construct that provides the complete regeneration of the functional tissue by fulfilling its common functions: barrier formation, defense against UV irradiation, thermoregulation, mechanical, and aesthetic functions [1].

A variety of cutaneous wounds is reported, each one resulting in its own distinctive healing approach: different devices have been developed to address specific clinical needs [5], ranging from passive solutions to tissue grafts. The former solutions support a large number of current medical procedures and are based on simple devices such as gauzes and bandages, whose primary function is to control the local microenvironment by protecting the wound from pathogenic infections. More sophisticated strategies are based on skin grafts: even if they represent the gold standard in large acute and chronic wounds [6], autograft and allograft availability can be scarce and more generally hold several limitations [1]. The use of dermal substitutes represents an effective alternative in improving the quality of wound healing [7] when compared to passive solutions. More advanced wound dressings, further promoting tissue healing via the delivery of biologically active agents or cells [8] from the dressing materials, have hence been proposed [6]. However, a significant degree of complexity is associated with these solutions, being based on fabrication processes with some limitations in scale-up, difficult management of both loading and controlled release of bioactive agents and cells, and significant costs [9].

Electrophoretic deposition (EPD) is a simple yet effective technology largely investigated for the biopolymer processing of a wide variety of coatings for biomedical applications [10], owing to its versatility in fine-tuning the properties of the processed biomaterials with a simple method of fabrication [11]. Such versatility can be further exploited using an innovative two-steps approach, electrophoretic replica deposition (EPrD) [12], in which deposited biopolymers are peeled from the working electrode by replicating the surface and morphology of the patterned substrate. EPrD has been successfully used to tailor both chemical composition and microstructure in several applications [12–14], showing its potential in manufacturing hierarchical supports for tissue regeneration, mainly made of chitosan.

Chitosan (CS) presents unique properties in terms of availability, handling, antibacterial and anti-inflammatory properties [15]. Next generation chitosan wound dressing can enhance wound progression towards healing by facilitating wound re-epithelialization and reducing the patient's pain level [16]. Chitosan's property of binding with red blood cells allows it to rapidly clot blood, making it effective in the treatment of severe hemorrhage [17]. In addition, chitosan modulates the response of inflammatory cells, subsequently promoting granulation and tissue organization [18]. Chitosan films, as a semipermeable biological dressing, maintain a sterile wound exudate beneath a dry scab, preventing dehydration and contamination of the wound and hence optimizing healing conditions. A clinical trial [16] demonstrated that chitosan dressings are able to reduce wound area and depth; moreover, chitosan seems to improve the management of wound exudates and reduce pain in dressing removal procedures.

In this work, we in vivo tested a family of chitosan patches fabricated by EPrD to evaluate the hypothesis that micro-patterned structures with precisely designed, open micro-channels might help dermal cells to reconstruct the skin. Due to the complexity of the skin tissue and the different layers constituting it, porous structures have been envisaged. Such structures can promote angiogenesis, manage wound exudates, and maintain a moist wound surface with open wound edges while insulating the wound, thus helping the control of bacterial loads. Random porosity and regularly oriented micro-channeled patches were fabricated via ErPD and thoroughly characterized to assess their physical and morphological

properties. A model of full thickness skin wounds allowed us to assess the ability to support in vivo tissue regeneration.

2. Materials and Methods

2.1. Materials

Chitosan (deacetylated chitin, poly(D-glucosamine) medium molecular weight, Lot#STBG1894V), acetic acid (99.7%), and water (CHROMASOLV® Plus, for HPLC) were all supplied by Sigma-Aldrich (Milan, Italy). Reagents were used as received and without further purification.

Three different aluminum sheets were used as cathodes in an electrophoretic deposition (EPD) cell: (i) flat substrates, to obtain patches with random porosity; (ii) micro-drilled sheets with regular lattices of circular holes of Φ = 500 μm (center to center distance 700 μm); (iii) micro-drilled sheets with regular lattices of circular holes of Φ = 1000 μm (center to center distance 1200 μm). (ii) and (iii) have been designed to obtain regular oriented micro-channeled patches.

Electrophoretic Replica Deposition

Electrodes were positioned at a distance of 10 mm [19] in a custom-made electrophoretic deposition cell. Processing conditions were optimized in order to achieve both the uniform, homogeneous, and consistent deposition of patches and the reproducibility of the patterns. Square waves (75–100 V, duty cycle = 0.17) were used in a water-based bath (pH = 3.38, (CS) = 1 g L^{-1}). The conductivity of the EPD bath was measured by a conductivity meter (Crison, CM 35, Hach Lange Spain, Barcelona, Spain).

Obtained patches were gently removed from the cathode after washing in deionized water: specimens were oven dried and stored until further characterization. Hereafter, chitosan patches will be indicated as *CPR* for random pore patches and *CP500* and *CP1000* for patches with regular oriented holes of Φ = 500 μm and Φ = 1000 μm, respectively.

2.2. Methods

2.2.1. Material Characterization

A scanning electron microscope (SEM, Zeiss EVO 50, accelerating voltage 20 kV, extended pressure mode) was used to assess the morphology of CS patches. The pore size dimensions were measured by means of ImageJ software (Rasband, W.S., ImageJ, US National Institutes of Health, Bethesda, MD, USA, http://imagej.nih.gov/ij/, 1997–2015) [20]. Two-dimensional pore distribution was plotted as pore diameter (supposed circular) *vs*. frequency. The thickness of the samples was evaluated by a confocal laser scanning microscope (Olympus LEXT OLS4100, Olympus, Tokio, Japan), 10X magnification BF Plan semi-apochromatic objective lens (MPLFLN10X, Olympus, Tokio, Japan). Mechanical properties were investigated on rectangular specimens (10 × 30 mm^2) by using an electromagnetic testing machine equipped with a 22 N load cell (ElectroForce 3200, TA Instruments, New Castle, DE, USA). Failure tensile tests were performed on the samples, at a crosshead speed of 0.2 min^{-1}, after 3 cycles of preconditioning up to 8% strain, performed at the same strain rate as failure tests. Selected strain rate is slightly lower, though in the same order of values, used by other authors to test chitosan [21]. Metal grips with a milled surface which avoids the slipping of the samples were used. The gripping force was manually regulated by a screw. Samples were immersed in PBS at 37 °C for 24 h before testing (mechanical tests were replicated on 5 samples for each CS patch.)

2.2.2. In Vivo Characterization

A full thickness skin wound (FTSW) animal model was tested in rats: all protocols were performed according to the Ethics Approval Committee of Ahvaz Jundishapur University of Medical Sciences (1394/657). The back areas of the rats were shaved and swabbed with 70% ethanol solution, under general anesthesia by ketamine/xylazine. A sterile square template (30 × 30 mm^2) was placed on the skin, and its boundaries were traced using a sterile fine felt-tipped pen. Then, an FTSW of the same size was made by excising the skin within the confines of the square down to the level of the subcutaneous panniculus carnosus. The wounds were then subjected to four different treatments (n = 5 for each group): (1) implantation of patches with flat morphology (CPR); (2) implantation of patches with 500 µm pore size (CP500); (3) implantation of patches with 1 mm pore size (CP1000); (4) untreated wounds (control). Patches were disinfected/sterilized by immersion in a 70% ethanol solution for 20 min. Patch skin grafts were then sutured over the wound and the wound site covered with a sterilized gauze and a biocompatible adhesive, LEUKOPLAST® ELASTOMULL® HAFT glue, was used. After the surgery, each animal was maintained in a cage: postsurgical care included analgesic and antibiotic injections. The appearance of any post-surgery complication was checked daily after surgery. After 14 days, rats in each group were euthanized by excessive dose of ketamine/xylazine and the reconstituted skin was evaluated.

Digital photographs of wound sites were acquired postoperatively on day 14 by a 10-megapixel digital camera (Panasonic DMC-FP3, Osaka, Japan) and analyzed with image software (Image J, http://rsb.info.nih.gov/ij/) by two blinded observers. In order to determine the differences in healing rate among the 4 groups, the wound closure percentage, *Wr* (%), was evaluated according to Equation (1):

$$Wr(\%) = 100 * \left(1 - \frac{A_{14}}{A_0}\right) \quad (1)$$

where A_0 is the wound area on postoperative day and A_{14} is the wound area after 14 days.

The reconstituted skin of all groups was excised to the level of panniculus carnosus layer, fixed in 10% formaldehyde, dehydrated, and then paraffin-embedded. Serial 10 µm paraffin sections were cut with a rotating microtome and stained with hematoxylin and eosin (H&E, kit from Asiapajouhesh, Tehran, Iran) and Masson's trichrome staining (Asiapajouhesh, Tehran, Iran), according to routine histological protocols.

The full thickness of the reconstituted skin was excised and fixed with 2.5% formaldehyde solution for 1 h to detect the expression level of keratin 10 (CK10) by immunohistochemistry. After dehydration by graded ethanol series (from 30% to 100%), the sample was embedded in a paraffin block to prepare tissue sections. Immunohistochemistry was performed according to the manufacturer's instructions. Briefly, a monoclonal anti-keratin 10 antibody (mouse IgG) (Abcam Inc., Cambridge, MA, USA) was incubated for 2 h and a secondary goat anti-mouse antibody (IgG) (1/1000) was subsequently incubated for 10 min. After extensive washes, the sample was incubated with 3,3'- diaminobenzidine until a brownish color appeared. The sample was counterstained with hematoxylin for 10 min.

2.3. Statistical Analysis

All results are reported as mean ± standard deviation. Significant differences between two sets of data were determined by one-way ANOVA followed by Tukey's post-hoc test for pairwise comparisons, and $p < 0.05$ was considered statistically significant (Minitab Express™ Version 1.4.0).

3. Results

3.1. Morphological Characterization

Figure 1a–c show the SEM micrographs of chitosan patches obtained via electrophoretic replica deposition. Figure 1d–f summarize the frequency and cumulative distributions of pore dimensions obtained by a quantitative analysis of SEM micrographs. Figure 1a reports the structure of patches obtained on flat cathodes. CPR specimens show a random porosity ranging between 10 and 300 μm: the cumulative distribution of pore diameter reveals that 75% of pores have a dimension of less than 150 μm (Figure 1d). Figure 1b,c show chitosan patches peeled from patterned cathodes: open, circular, and spatially regular micro-channels with diameters of ≈ 500 μm and 1000 μm are evident on CP500 (Figure 1b) and CP1000 (Figure 1c), respectively. A secondary random porosity with spherical pores is also evident and is confirmed by the frequency distribution of pores. It is worth of notice that the frequency of microchannels in the distribution plot is apparently low; however, being the distribution based on the number of the pores, it appears evident that the lower numerosity (Figure 1e,f) is coherent with the spatial distribution of the lattice (Figure 1a–c). The obtained microchannels do not show cracks or other defects, appearing clearly defined. The thickness has been evaluated for all the patches via confocal laser microscopy (see SI1): patches showed a thickness in the range of 230 ± 25 μm (patterned) and 250 ± 25 μm (flat), with no significant difference among the three groups.

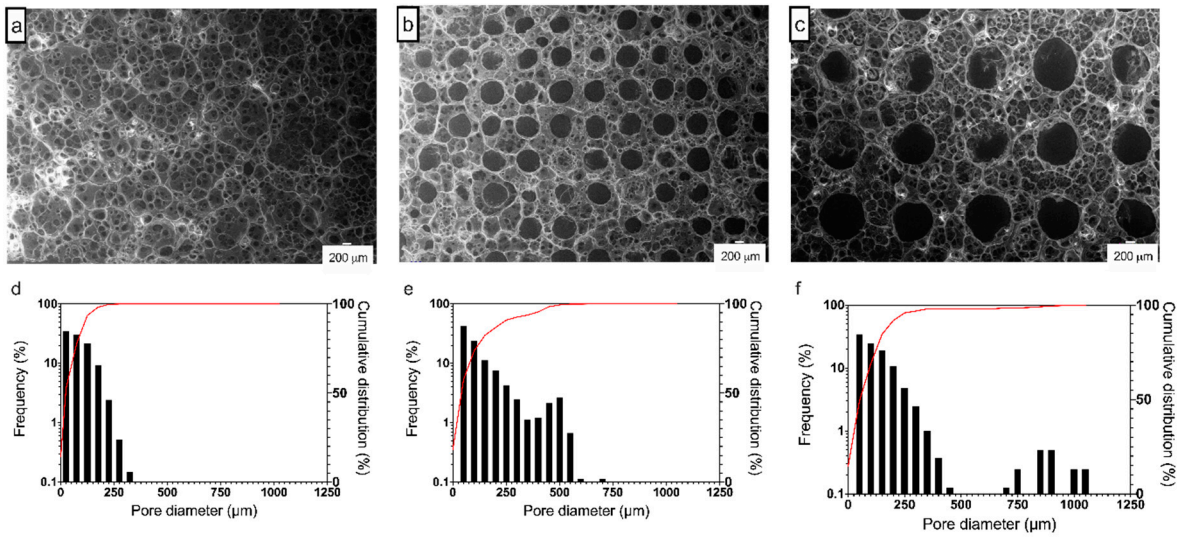

Figure 1. (**a**–**c**) Representative SEM micrographs and (**d**–**f**) frequency and cumulative distributions of pore dimension of (**a**,**d**) CPR, (**b**,**e**) CP500, and (**c**,**f**) CP1000 electrophoretic replica deposition (EPrD) chitosan patches. (SEM scale bar 200 μm.)

3.2. Mechanical Properties

Tensile tests have been performed after three cycles of preconditioning up to 8% strain. This preconditioning allows an understanding of the viscoelastic behavior of the material: a negligible hysteresis was observed for both flat (CPR, Figure 2a) and patterned samples (SI2). Preconditioning is required when testing soft viscoelastic materials in order to achieve repeatable results. Preliminary tests on our scaffolds showed the low effect of strain rate on the stress–strain slope, confirmed by the low number (2) of precondition cycles needed to obtain repeatable results and by the negligible hysteresis area.

Stress–strain curves show a characteristic pure elastic behavior for all the wet materials (Figure 2b). All the chitosan patches showed a similar stress at break (near 0.5 MPa) and deformation at break between

30% and 40%, with no significant differences among the samples (Figure 2b). Figure 2c reports the Young's modulus of CS patches: a slight decrease can be observed from CPR to CP1000 patches (no significant difference detected among the three different structures).

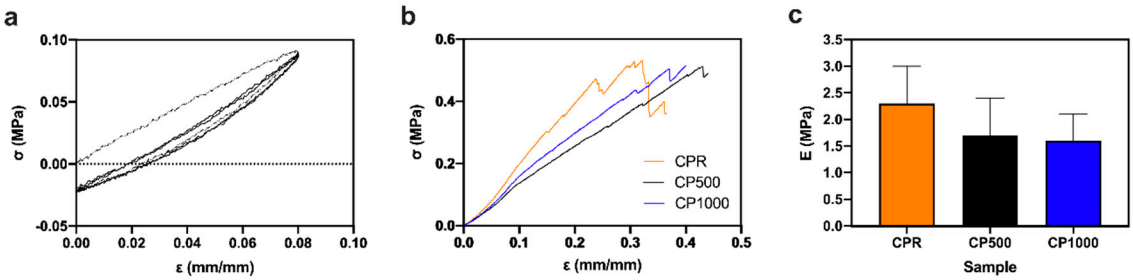

Figure 2. Uniaxial tensile tests on flat and micro-patterned patches in wet conditions: (**a**) representative preconditiong cycle for CPR specimens, (**b**) tensile tests up to break, and (**c**) Young modulus (E).

3.3. In Vivo Tests

No postoperative adverse effects, such as infection, pyogenesis, and body fluid effusions, occurred in any animal: diet, drinking, and defecation were normal throughout the experiment. On day 0, a full thickness skin wound of 30 × 30 mm^2 was made in every group: Figure 3a shows the typical implant sites at day 0, immediately after full thickness skin wound (FTSW) preparation. Figure 3b–d show the appearance of the representative wound sites in the different groups at day 14: chitosan patches, regardless of their structure, promoted wound healing from day 1 to 14. On day 14, hairs were grown on the surrounding area of the un-epithelialized wound in all groups. To take photographs of the un-epithelialized wound area, the surrounding hairs were re-shaved to clearly show the wound margins.

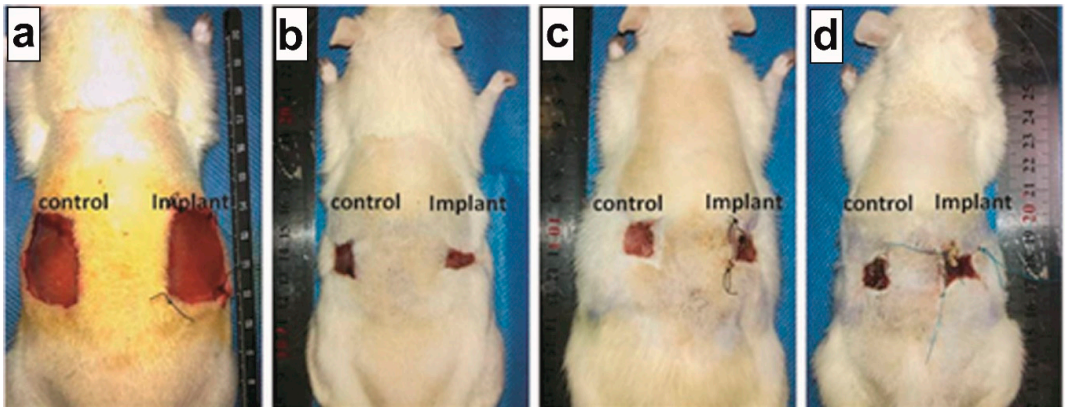

Figure 3. Wound sizes at (**a**) day 0 and (**b**–**d**) after 14 days of implantation. (**b**) CPR wound rate (WR) after 14 days, WR = 89%; (**c**) CP500 WR = 87%; (**d**) CP1000 WR = 81%; (**b**–**d**) specimens are compared with non-treatment condition (control), showing WR = 81%.

On day 14, the largest un-epithelialized wound was found in the CP1000 group, followed by the CPR and CP500 groups. A reduction in wound size has been observed for all the samples (Figure 3b–d): a significant difference has been observed between CPR samples (WR 89%) vs. non-treatment control condition (81%) and between CP500 (WR 87%) vs. non-treatment control condition (81%). No differences have been observed between CP1000 and non-treatment control condition of 81% in either sample.

Histological staining of wound areas at day 14 is reported in Figure 4. On day 14, necrotic fibrinoid debris (FD), inflammatory infiltration, fibroblast, and capillary (CP, Figure 5) hyperproliferation were

still observed in the CP1000 group, indicating a still persistent inflammation process for this group (Figure 4, CP1000). Wounds in CPR and CP500 groups demonstrated epithelialization (EP) without capillary hyperplasia. Compared with normal skin, more layers of keratinocytes were seen in CPR and CP500 groups, indicating the proliferating stage of keratinocytes in these two groups. A thin epidermal layer with several skin appendages, including hair follicles (HF) and sebaceous glands (SB), were shown in the CPR group as compared to CP500 and CP1000 groups (Figure 4). Moreover H&E and Masson's trichrome staining showed an important inflammatory infiltrate present only on CP1000, where a significant amorphous fibrotic mass is also present. Moreover, the extracellular matrix appears still not organized, while CPR showed granular and cornified layers and cutaneous annex formation (hair follicles, sebaceous glands), comparable with controls. CP500 also shows the epithelial layers and the presence of cutaneous annexes (Figure 4).

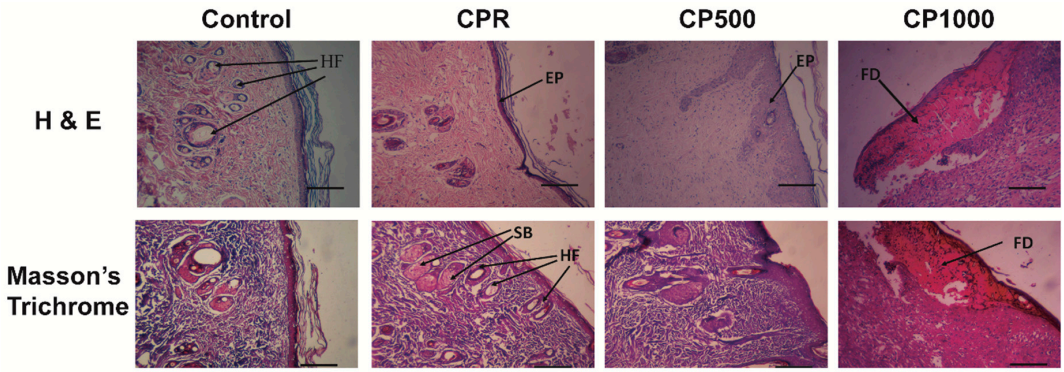

Figure 4. Hematoxylin and eosin and Masson's trichrome staining in different groups on day 14. FD, fibrinous debris; EP, epithelialization; HF, hair follicle; SB, sebaceous gland. (Scale bar = 50 μm.).

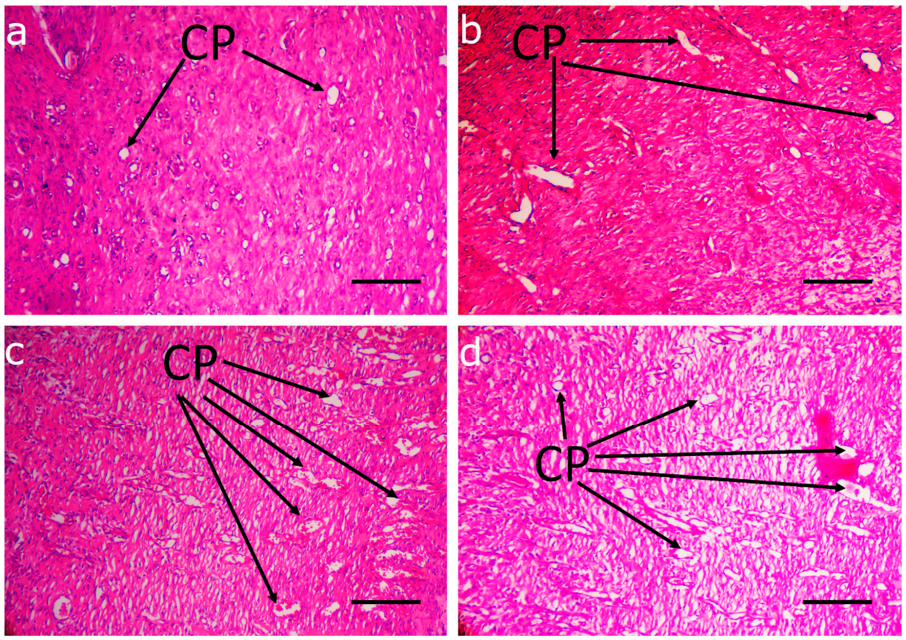

Figure 5. Capillary formation in deep dermal layers of different implantation groups on day 14. (**a**) CPR; (**b**) CP500; (**c**) CP1000; (**d**) control. Capillary hyperplasia (arrows) was markedly observed in CP1000 group and in control group. Scale bar: 30 μm.

In addition, coarse bundles of collagen were observed in the dermis for CPR and CP500 groups, as stained with Masson's technique, whereas reticular fibers and thin collagen bundles were mostly observed for the CP1000 group, as shown by silver staining (SI3). Furthermore, immunohistochemical studies demonstrated that CK10 was uniformly expressed in the epithelium of the CP1000 group, whereas it was mostly expressed in the basal and suprabasal layers of CPR and CP500 groups (Figure 6), confirming a mature tissue structure in these latter samples.

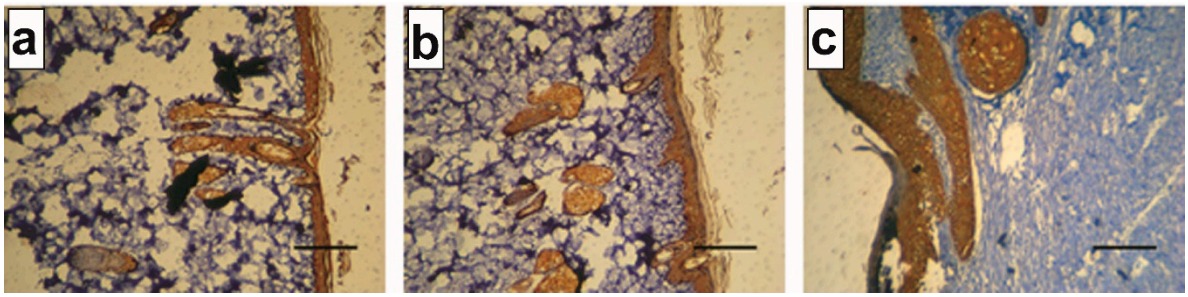

Figure 6. Immunohistochemical analysis against keratin 10 (CK10) at day 14 on (**a**) CPR, (**b**) CP500, and (**c**) CP1000. (Scale bar 50 μm.)

Moreover, after tissue processing and histological examination, there is no sign of chitosan in regenerated skin. It seems that chitosan scaffolds were completely replaced by newly formed reticular and collagen fibers.

4. Discussion

In the last decade, the study of so-called bioactive dressings has been actively promoted [22]. Such devices are based on the use of naturally occurring proteins and polysaccharides that possess a notable biocompatibility and allow the dressing to achieve the highest level of biomimicry, recapitulating the native extracellular matrix (ECM) biological and physico-chemical features [23–25]. In this work, we have shown the use of the electrophoretic replica deposition technique as an innovative technology to simply manufacture bioactive dressings that can promote wound healing via the fine-tuning of their microstructure and an appropriate choice of material. This new family of structures was shown to support skin wound healing in large defects via an in vivo rat model.

Figure 7 schematically illustrates the EPrD technology process diagram and the possible achievable material properties. EPD is a conventional electrophoretic process originally designed for surface modifications and largely exploited in several industrial applications to impart specific properties to material surfaces [11]. EPrD is an EPD process characterized by the subsequent mechanical or chemical removal of the deposited material from the working electrode. Through a machining technology (e.g., drilling, laser-cut), it is possible to impart a microstructure to the working electrode: such patterns will be hence replicated on the surface of the deposit by controlling EPD processing parameters. Moreover, complex three-dimensional shapes (such as tubes) can be replicated, allowing to obtain the manufacturing of objects at different scales, from fine-tuned compositions at nano-scale up to cm-scale devices (right box in Figure 7).

Almost all the potentials offered by this technology have been exploited here in order to obtain structures suitable for skin wound management. Namely, through the correct selection of the composition of the deposition bath, the micro-structuring of the deposition substrate, and the process parameters, it was possible to manufacture in a consistent way a family of hierarchical patches (Figure 1). EPrD allowed the easy and consistent processing of chitosan: this biopolymer has been selected as material to design

bioactive dressings based on both the wide literature related to its processing via EPD [10] and its ability to promote hemostasis, accelerate tissue regeneration, and stimulate the fibroblast synthesis of collagen [26–29]. Previous studies demonstrated that chitosan accelerates wound healing due to the infiltration of polymorphonuclear (PMN) cells at the wound site [30], which is a crucial event in rapid wound healing. The EPrD process also enabled the obtainment of hierarchical structures with controlled morphology and thickness: porous polymer structures are of increasing interest due to their wide application as scaffolds for tissue regeneration as well as immune-isolating membrane [24,25,31]. The microstructure of the porous patches, such as the pore shape, pore size, and pore distribution, has been easily tailored by combining the micro-structuring of the cathode substrate and exploiting the intrinsic effect of hydrogen gas development due to the water electrolysis [32,33], the latter resulting in this work in a secondary random porosity in the range of 10–100 µm (Figure 1).

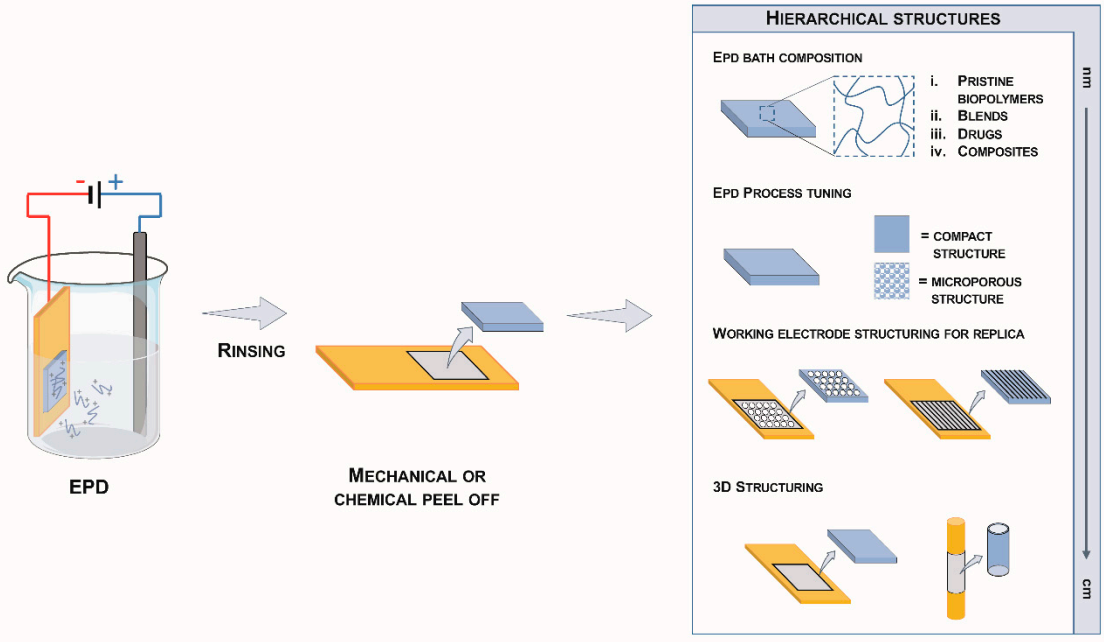

Figure 7. Scheme of the electrophoretic replica deposition process (EPrD).

EPrD allowed us to obtain CS porous patches with a thickness of around 230 µm, suitable for dermal regeneration [34]. In contrast to autografts, dermal substitutes suffer from a lack of normal vascular networks: a suitable thickness is then needed for oxygen and nutrient diffusion. Impaired diffusion processes due to thick scaffolds result in tissue necrosis, extensive inflammatory reaction, marked foreign-body reaction (FBR), and rapid scaffold degradation [34]. In contrast, thinner scaffolds, especially those with a thickness of less than 0.5 mm, promote earlier angiogenesis, ensuring skin-graft viability with a mild FBR, ordered fibroblast infiltration, and better collagen remodeling [12,34]. It is worth mentioning that the application of nanofibrous mats with a thickness of 500 µm can accelerate wound healing by around one week in rats [35].

Finally, the EPrD technique allowed us to obtain structures showing mechanical properties suitable to support protective functions and maintain the elastic properties of the skin during wound healing, with elastic behavior and a strain at break of up to 40%. The Young's modulus of the samples was comparable to that found by Haifei et al. [34] and in the range of elastic modulus in normal human skin (E = 0.2–20 MPa), indicating the acceptable mechanical strength and elasticity of these patches and making them suitable for in vivo grafting [36]. Altogether, these results support the use of the obtained chitosan

patches as dermal templates for the treatment of skin defects using a one-stage grafting procedure in a full thickness wound skin model in rats. Previous studies demonstrated that CS has an anti-inflammatory and antimicrobial nature [14,37] and can accelerate wound healing [38]. Some authors found that chitosan promotes the contraction and epithelialization of wounds by means of facilitating the migration and proliferation of epithelial cells and myofibroblasts [38].

In this work, the efficacy of chitosan patches in large wound sites has been assessed in vivo. Ethanol disinfection was used prior to implantation. Disinfection techniques, particularly the use ethanol, are widely applied in the development of novel biomaterials prior to in vitro testing [39]. Ethanol solutions (60–90% in water) are known to possess bactericidal properties [39]. Some authors define the ethanol soaking of scaffolds as a sterilization technique [40], even though there are concerns about the efficacy of ethanol disinfection for implanted biomaterials [41]. However, ethanol solutions are used by some authors prior to in vivo implantation when other sterilization techniques can alter the physical or chemical structure of the scaffolds or their degradation profiles [12,41,42]. In our study, no postoperative adverse effects such as infection, pyogenesis, and body fluid effusion occurred in any animals throughout the experimental period. More importantly, it is worth noting that the FTWS of 900 mm^2 reported here is higher than in previous studies on chitosan showing re-epithelialization at 14 days, with an FTWS ranging from 20 mm^2 to 150 mm^2 [38,43–46]. In all cases, the wound sites were significantly lower than the case reported here. Histological sections found a thin epidermal layer similar to normal skin. More skin appendages, including hair follicles (HF) and sebaceous glands (SB), were formed in the CPR group as compared to CP500 and CP1000 groups for 14 days. Immunohistochemistry demonstrated that keratin 10 (CK10) was uniformly expressed in the epithelium of the CP1000 group, whereas it was mostly expressed in the basal and suprabasal layers of CPR and CP500 groups, like normal skin. The wound contraction observed 14 days after implantation seemed to be very high for all types of patches, especially CPR and CP500, considering that the initial scar dimensions were higher than those presented in many other studies [44,45,47].

Random structure (CPR) and hierarchical structure with lower dimensions (CP500) seem to better support the migration and proliferation of fibroblasts from peripheral zones in proximity to the wound as compared to chitosan porous patches with larger channels (CP1000). Both the pore size and the structure of the scaffold are key points influencing cell interaction and migration. However, it is difficult to draw general conclusions on the specific pore size for skin regeneration, the tissue being constituted by different types of cells in its layers. The excellent recent review by Haugen and coworkers [48] can help to elucidate this point. The epidermis is mainly constituted by keratinocytes (95%), but also by Langerhans, melanocytes, Merkel–Ranvier, and inflammatory cells; the dermis contains fibroblasts, macrophages, adipocytes, blood vessels, and nerve receptors. Following on from this, a 5-μm pore size has been reported to be suitable for neovascularization, 5–15-μm for fibroblast ingrowth, and 20–125-μm for dermal repair [48]. The present studies, and the results obtained mainly with the CPR and CP500 specimens, confirmed that a distribution of micropore dimensions with a cumulative distribution in which the large sections of pores have a dimension of less than 150 μm was able to support neovascularization, fibroblast ingrowth, and dermal repair. Moreover, numerous systemic and local factors are involved in the wound healing process, such as cellular adhesion, migration, proliferation, differentiation, and apoptosis [49]. In fact, the migration rate of fibroblasts can be quite fast (up to 200 μm/day), but these cells only produce ECM if the blood vessels and nutrients are within 100 μm [48]. Hence, angiogenesis represents the main rate-limiting step: we decided to set the distances between channels at 200 μm. The presence of a lattice of microchannels did not evidence a specific advantage in the case of CP500; however, based on previous findings [12], a significant difference in supporting the presence of highly neo-vascularized tissue, inside and around scaffolds, with precisely-designed, regularly-spaced, open micro-channels that pass through the scaffold and contact the microporous structure, can be evidenced at later stages at longer implantation periods.

A growing body of evidence supports the hypothesis that the neo-vascularization of porous structures can be modulated by the design of such structures containing continuous networks [12]. Additionally, the typical thickness of the specimens could support the positive overall response of the patches, even in the absence of microchannels.

Finally, the CP1000 specimen results could support the hypothesis that there should be a critical upper dimension of microchannels; however, further studies could elucidate the differences arising from the hierarchical structure, range of dimensions, stability of the scaffolds, and their thickness.

5. Conclusions

The potential of using the electrophoretic replica deposition technique to fabricate chitosan patches with hierarchical structures for wound management has been reported in this study. An optimized EPD process allowed us to obtain micro-structured chitosan patches via a replica of the cathode substrate in a simple yet effective and consistent way: the obtained morphology and mechanical properties appear suitable for the target tissue. In vivo studies showed enhanced performance of the EPrD patches by inducing fast re-epithelialization and wound closure. Collectively, these results show the potential of the EPrD technology in designing advanced substrates for the treatment of large full thickness skin wounds based on micro-structured chitosan.

Supplementary Materials: The following are available online at http://www.mdpi.com/2076-3417/10/14/5010/s1, SI1: Confocal Laser Microscopy, SI2: Preconditioning mechanical tests, SI3: Silver Staining.

Author Contributions: Conceptualization, L.A., L.D.N., V.B.; methodology, F.B. (Federica Boschetti), L.A., V.B., L.D.N.; validation, A.G.E., F.N., L.B., F.B. (Francesca Boccafoschi); formal analysis, A.G.E., L.A., F.B. (Federica Boschetti); data curation, F.B. (Federica Boschetti), L.D.N., F.N.; writing—original draft preparation, A.G.E., F.N., L.A.; writing—review and editing, F.B. (Federica Boschetti), L.D.N., L.B., V.B. F.B. (Francesca Boccafoschi); supervision, L.D.N., R.C.; funding acquisition, L.D.N., V.B., R.C. All authors have read and agreed to the published version of the manuscript.

Funding: This research received no external funding.

Conflicts of Interest: The authors declare no conflict of interest.

References

1. Metcalfe, A.D.; Ferguson, M.W.J. Tissue Engineering of Replacement Skin: The Crossroads of Biomaterials, Wound Healing, Embryonic Development, Stem Cells and Regeneration. *J. R. Soc. Interface* **2007**, *4*, 413–437. [CrossRef]
2. Clark, R.A.F.; Ghosh, K.; Tonnesen, M.G. Tissue Engineering for Cutaneous Wounds. *J. Investig. Dermatol.* **2007**, *127*, 1018–1029. [CrossRef]
3. Gurtner, G.C.; Werner, S.; Barrandon, Y.; Longaker, M.T. Wound Repair and Regeneration. *Nature* **2008**, *453*, 314–321. [CrossRef]
4. Basu, P.; Narendrakumar, U.; Arunachalam, R.; Devi, S.; Manjubala, I. Characterization and Evaluation of Carboxymethyl Cellulose-Based Films for Healing of Full-Thickness Wounds in Normal and Diabetic Rats. *ACS Omega* **2018**, *3*, 12622–12632. [CrossRef] [PubMed]
5. Mir, M.; Ali, M.N.; Barakullah, A.; Gulzar, A.; Arshad, M.; Fatima, S.; Asad, M. Synthetic Polymeric Biomaterials for Wound Healing: A Review. *Prog. Biomater.* **2018**, *7*, 1–21. [CrossRef] [PubMed]
6. Abdel-Sayed, P.; Hirt-Burri, N.; de Buys Roessingh, A.; Raffoul, W.; Applegate, L.A. Evolution of Biological Bandages as First Cover for Burn Patients. *Adv. Wound Care* **2019**, *8*, 555–564. [CrossRef] [PubMed]
7. Yannas, I.V.; Orgill, D.P.; Burke, J.F. Template for Skin Regeneration. *Plast. Reconstr. Surg.* **2011**, *127* (Suppl. S1), 60S–70S. [CrossRef]

8. Draghi, L.; Brunelli, D.; Farè, S.; Tanzi, M.C. Programmed Cell Delivery from Biodegradable Microcapsules for Tissue Repair. *J. Biomater. Sci. Polym. Ed.* **2015**, *26*, 1002–1012. [CrossRef]
9. Blacklow, S.O.; Li, J.; Freedman, B.R.; Zeidi, M.; Chen, C.; Mooney, D.J. Bioinspired Mechanically Active Adhesive Dressings to Accelerate Wound Closure. *Sci. Adv.* **2019**, *5*, eaaw3963. [CrossRef]
10. Avcu, E.; Baştan, F.E.; Abdullah, H.Z.; Rehman, M.A.U.; Avcu, Y.Y.; Boccaccini, A.R. Electrophoretic Deposition of Chitosan-Based Composite Coatings for Biomedical Applications: A Review. *Prog. Mater. Sci.* **2019**, *103*, 69–108. [CrossRef]
11. De Nardo, L.; Altomare, L.; De Curto, B.; Cigada, A.; Draghi, L. Electrochemical Surface Modifications of Titanium and Titanium Alloys for Biomedical Applications. In *Coatings for Biomedical Applications*; Woodhead Publishing: Cambridge, UK, 2012; pp. 106–142. [CrossRef]
12. Varoni, E.M.; Altomare, L.; Cochis, A.; Ghalayaniesfahani, A.; Cigada, A.; Rimondini, L.; De Nardo, L. Hierarchic Micro-Patterned Porous Scaffolds via Electrochemical Replica-Deposition Enhance Neo-Vascularization. *Biomed. Mater.* **2016**, *11*. [CrossRef]
13. Esfahani, A.G.; Soleimanzade, M.; Campiglio, C.E.; Federici, A.; Altomare, L.; Draghi, L.; Boccaccini, A.R.; De Nardo, L. Hierarchical Microchannel Architecture in Chitosan/Bioactive Glass Scaffolds via Electrophoretic Deposition Positive-Replica. *J. Biomed. Mater. Res. Part A* **2019**. [CrossRef]
14. Ghalayani Esfahani, A.; Altomare, L.; Varoni, E.M.; Bertoldi, S.; Farè, S.; De Nardo, L. Electrophoretic Bottom up Design of Chitosan Patches for Topical Drug Delivery. *J. Mater. Sci. Mater. Med.* **2019**, *30*, 1–8. [CrossRef]
15. Dash, M.; Chiellini, F.; Ottenbrite, R.M.; Chiellini, E. Chitosan—A Versatile Semi-Synthetic Polymer in Biomedical Applications. *Prog. Polym. Sci. (Oxf.)* **2011**. [CrossRef]
16. Mo, X.; Cen, J.; Gibson, E.; Wang, R.; Percival, S.L. An Open Multicenter Comparative Randomized Clinical Study on Chitosan. *Wound Repair Regen.* **2015**, *23*, 518–524. [CrossRef]
17. Kozen, B.G.; Kircher, S.J.; Henao, J.; Godinez, F.S.; Johnson, A.S. An Alternative Hemostatic Dressing: Comparison of CELOX, HemCon, and QuikClot. *Acad. Emerg. Med.* **2008**, *15*, 74–81. [CrossRef] [PubMed]
18. Ueno, H. Topical Formulations and Wound Healing Applications of Chitosan 2. Topical Findings of Healing with Chitosan at Early Phase of Experimental Open Skin Wound. *Adv. Drug Deliv. Rev.* **2001**, *52*, 105–115. [CrossRef]
19. Isfahani, A.G.; Ghorbani, M. Electrophoretic Deposition of Ni/SiO_2 Nanocomposite Coating: Fabrication Process and Tribological and Corrosion Properties. *J. Nano Res.* **2013**, *26*, 45–51. [CrossRef]
20. Bartoš, M.; Suchý, T.; Foltán, R. Note on the Use of Different Approaches to Determine the Pore Sizes of Tissue Engineering Scaffolds: What Do We Measure? *Biomed. Eng. Online* **2018**, *17*, 110. [CrossRef]
21. Sarasam, A.; Madihally, S.V. Characterization of Chitosan-Polycaprolactone Blends for Tissue Engineering Applications. *Biomaterials* **2005**. [CrossRef]
22. Dhivya, S.; Padma, V.V.; Santhini, E. Wound Dressings—A Review. *BioMedicine* **2015**, *5*, 22. [CrossRef] [PubMed]
23. Suarato, G.; Bertorelli, R.; Athanassiou, A. Borrowing From Nature: Biopolymers and Biocomposites as Smart Wound Care Materials. *Front. Bioeng. Biotechnol.* **2018**, *6*. [CrossRef] [PubMed]
24. Campiglio, C.E.; Negrini, N.C.; Farè, S.; Draghi, L. Cross-Linking Strategies for Electrospun Gelatin Scaffolds. *Materials* **2019**, *12*, 2476. [CrossRef] [PubMed]
25. Emma Campiglio, C.; Marcolin, C.; Draghi, L. Electrospun ECM Macromolecules as Biomimetic Scaffold for Regenerative Medicine: Challenges for Preserving Conformation and Bioactivity. *AIMS Mater. Sci.* **2017**, *4*, 638–669. [CrossRef]
26. Taravel, M.N.; Domard, A. Collagen and Its Interaction with Chitosan. II. Influence of the Physicochemical Characteristics of Collagen. *Biomaterials* **1995**, *16*, 865–871. [CrossRef]
27. Taravel, M.N.; Domard, A. Collagen and Its Interactions with Chitosan: III. Some Biological and Mechanical Properties. *Biomaterials* **1996**, *17*, 451–455. [CrossRef]
28. Cho, Y.-W.; Cho, Y.-N.; Chung, S.-H.; Yoo, G.; Ko, S.-W. Water-Soluble Chitin as a Wound Healing Accelerator. *Biomaterials* **1999**, *20*, 2139–2145. [CrossRef]

29. Ma, J.; Wang, H.; He, B.; Chen, J. A Preliminary in Vitro Study on the Fabrication and Tissue Engineering Applications of a Novel Chitosan Bilayer Material as a Scaffold of Human Neofetal Dermal Fibroblasts. *Biomaterials* **2001**, *22*, 331–336. [CrossRef]
30. Ueno, H.; Yamada, H.; Tanaka, I.; Kaba, N.; Matsuura, M.; Okumura, M.; Kadosawa, T.; Fujinaga, T. Accelerating Effects of Chitosan for Healing at Early Phase of Experimental Open Wound in Dogs. *Biomaterials* **1999**, *20*, 1407–1414. [CrossRef]
31. Widmer, M.S.; Mikos, A.G. Fabrication of Biodegradable Polymer Scaffolds for Tissue Engineering. In *Frontiers in Tissue Engineering*; Pergamon Elsevier: Oxford, UK, 1998; pp. 107–120. [CrossRef]
32. Simchi, A.; Pishbin, F.; Boccaccini, A.R. Electrophoretic Deposition of Chitosan. *Mater. Lett.* **2009**, *63*, 2253–2256. [CrossRef]
33. Altomare, L.; Draghi, L.; Chiesa, R.; De Nardo, L. Morphology Tuning of Chitosan Films via Electrochemical Deposition. *Mater. Lett.* **2012**, *78*, 18–21. [CrossRef]
34. Haifei, S.; Xingang, W.; Shoucheng, W.; Zhengwei, M.; Chuangang, Y.; Chunmao, H. The Effect of Collagen—Chitosan Porous Scaffold Thickness on Dermal Regeneration in a One-Stage Grafting Procedure. *J. Mech. Behav. Biomed. Mater.* **2014**, *29*, 114–125. [CrossRef] [PubMed]
35. Nejaddehbashi, F.; Hashemitabar, M.; Bayati, V.; Abbaspour, M.; Moghimipour, E.; Orazizadeh, M. Application of Polycaprolactone, Chitosan, and Collagen Composite as a Nanofibrous Mat Loaded with Silver Sulfadiazine and Growth Factors for Wound Dressing. *Artif. Organs* **2019**, *43*, 413–423. [CrossRef] [PubMed]
36. Joodaki, H.; Panzer, M.B. Skin Mechanical Properties and Modeling: A Review. *Proc. Inst. Mech. Eng. Part H J. Eng. Med.* **2018**, *232*, 323–343. [CrossRef]
37. Ghalayani Esfahani, A.; Lazazzera, B.; Draghi, L.; Farè, S.; Chiesa, R.; De Nardo, L.; Billi, F. Bactericidal Activity of Gallium-Doped Chitosan Coatings against Staphylococcal Infection. *J. Appl. Microbiol.* **2019**, *126*, 87–101. [CrossRef]
38. Abdulaziz, S.S.; Gabr, G.A.; Soliman, G.A.; Fayed, M.H.; Ansari, M.N. The Potential Anti-Inflammatory and Wound Healing Activities of Rats. *Adv. Biores.* **2016**, *7*, 1–7. [CrossRef]
39. Horakova, J.; Klicova, M.; Erben, J.; Klapstova, A.; Novotny, V.; Behalek, L.; Chvojka, J. Impact of Various Sterilization and Disinfection Techniques on Electrospun Poly-ε-Caprolactone. *ACS Omega* **2020**, *5*, 8885–8892. [CrossRef] [PubMed]
40. Dai, Z.; Ronholm, J.; Tian, Y.; Sethi, B.; Cao, X. Sterilization Techniques for Biodegradable Scaffolds in Tissue Engineering Applications. *J. Tissue Eng.* **2016**, *7*, 2041731416648810. [CrossRef]
41. Huebsch, N.; Gilbert, M.; Healy, K.E. Analysis of Sterilization Protocols for Peptide-Modified Hydrogels. *J. Biomed. Mater. Res. Part B Appl. Biomater.* **2005**, *74B*, 440–447. [CrossRef] [PubMed]
42. Lynn, A.D.; Kyriakides, T.R.; Bryant, S.J. Characterization of the In Vitro Macrophage Response and In Vivo Host Response to Poly(Ethylene Glycol)-Based Hydrogels. *J. Biomed. Mater. Res. Part A* **2010**, *93A*, 941–953. [CrossRef]
43. Ahmed, S.; Ikram, S. Chitosan Based Scaffolds and Their Applications in Wound Healing. *Achiev. Life Sci.* **2016**, *10*, 27–37. [CrossRef]
44. Cahú, T.B.; Silva, R.A.; Silva, R.P.F.; Silva, M.M.; Arruda, I.R.S.; Silva, J.F.; Costa, R.M.P.B.; Santos, S.D.; Nader, H.B.; Bezerra, R.S. Evaluation of Chitosan-Based Films Containing Gelatin, Chondroitin 4-Sulfate and ZnO for Wound Healing. *Appl. Biochem. Biotechnol.* **2017**, *183*, 765–777. [CrossRef]
45. Hajji, S.; Khedir, S.B.; Hamza-Mnif, I.; Hamdi, M.; Jedidi, I.; Kallel, R.; Boufi, S.; Nasri, M. Biomedical Potential of Chitosan-Silver Nanoparticles with Special Reference to Antioxidant, Antibacterial, Hemolytic and In Vivo Cutaneous Wound Healing Effects. *Biochim. Biophys. Acta(BBA)-Gen. Subj.* **2019**, *1863*, 241–254. [CrossRef]
46. Song, X.; Mei, J.; Zhang, X.; Wang, L.; Singh, G.; Xing, M.M.Q.; Qiu, X. Flexible and Highly Interconnected, Multi-Scale Patterned Chitosan Porous Membrane Produced in Situ from Mussel Shell to Accelerate Wound Healing. *Biomater. Sci.* **2017**, *5*, 1101–1111. [CrossRef] [PubMed]
47. Archana, D.; Dutta, J.; Dutta, P.K. Evaluation of Chitosan Nano Dressing for Wound Healing: Characterization, In Vitro and In Vivo Studies. *Int. J. Biol. Macromol.* **2013**, *57*, 193–203. [CrossRef] [PubMed]

48. Rahmati, M.; Blaker, J.J.; Lyngstadaas, S.P.; Mano, J.F.; Haugen, H.J. Designing Multigradient Biomaterials for Skin Regeneration. *Mater. Today Adv.* **2020**. [CrossRef]
49. Tavaria, F.; Jorge, M.P.; Ruiz, L.T.; Pintado, M.E.; Carvalho, J.E. Anti-Proliferative, Anti-Inflammatory, Anti-Ulcerogenic and Wound Healing Properties of Chitosan. *Curr. Bioact. Compd.* **2016**, *12*, 114–122. [CrossRef]